SUPPORTING INFORMATION

Supramolecular self-assembly in sub-micron electrodic cavity: fabrication of heat reversible π-gel memristor

By Lei ZHANG, Songlin LI, Marco A. SQUILLACI, Xiaolan ZHONG, Yifan YAO, Emanuele ORGIU and Paolo SAMORI**

Table of Contents

1. Experimental section

1.1 Materials:

Lithium fluoride (LiF, 99.995%), toluene (anhydrous; 99.8%), regioregular P3HT (Mw, 55000) and regiorandom P3HT (Mw, 70000-90000) are all purchased from Sigma-Aldrich and used as received without further purification. Regioregular P3HT (Mw=31300) is purchased from Ossila and used as received. Patterned ITO substrates and bare glass substrates are both purchased from Luminescence Technology Corporation.

1.2 The fabrication of cavity electrodes:

Substrate preparation. The glass and ITO-glass substrates were received from Luminescence Technology Corporation and have been cut into 1.5 × 2.0 cm^2 and 1.5 × 1.2 cm^2. The thickness of the glass substrate is 0.7 mm. Before device fabrication, glass substrates were thoroughly rinsed with NaOH aqueous solution (5 w%) and deionized water in sequence, then substrates were dried with nitrogen flow.

Gold layer and LiF pillars array deposition. Clean glass substrates were transferred in a vacuum chamber to thermally evaporate a thin layer of 2 nm of Cr, followed by 10 nm of Au. Then a photo resist AZ 1505 was spin-coated onto the glass substrate at a spin speed of 3000 rpm. After exposure and development process, Au/Cr electrodes were obtained by wet etching. Thereafter, 260 nm Au pads were deposited through a shadow mask to define the region where cold welding would occur (Figure 2a in the main text). Before cold-welding, a 500 nm LiF pillars array was patterned at the pre-designed device region by photolithography. The cold-welding process was performed using a hydraulic press machine.

2. Electrical measurement conditions:

Figure 4a in the main text: Scan the voltage from 0 V to 4 V and record the current through pure anhydrous toluene, freshly prepared regioregular P3HT solution and regiorandom P3HT solution. The latter two kinds of polythiophene solution exhibit the same concentration of 25 mg/ml in toluene. "Fresh solution" means the solution is prepared by heating it up to 85 ^{o}C for 30 minutes and then cooling down to room temperature (approx. 21 ^{o}C to 22 ^{o}C). The electrical measurement was performed at room temperature using a Keithley 2636 sourcemeter.

Figure 4b in the main text: Scan the voltage from 0 V to 4 V and control the temperature by a hotplate. Every time when the hotplate reached a certain temperature, we would stand by at least 15 minutes before the *I-V* scanning. The measurement prototype has been shown in Figure 2c.

Figure 4c in the main text: The voltage bias and reading process were controlled by a Labview program home-written for Keithley 2636 sourcemeter. In detail, we applied a 10 seconds period of 4 V DC bias, then stand by 0.5 s before recording the current at 4 V voltage.

Figure 4d in the main text: The measurement recipe was similar to Figure 4c, but the main difference lies that the duration of DC bias voltage, i.e., the interval between two reading process, has been prolonged to 200 seconds. And the reading pulse at 1 V has been shorten to 100 ms to avoid the interference by measurement.

Figure 5a: The measurement recipe was also similar to Figure 4c with the interval between two times of measurement has been set to be 5 seconds. The bias voltage was kept 4 V. "Aged" solution was prepared by storing the "fresh" solution at room temperature for 24 hours. The "gel" sample was obtained by putting the device into fridge (ca. 4 ^{o}C) for more than 30 minutes. Before the electrical measurement, the gel device has been kept outside of the fridge for 1 hour to let it warm up to room temperature (approx. 21 ^{o}C to 22 ^{o}C). This measurement condition has also been applied in the case of Figure S12d, 12e and Figure S14a where "room temperature (22 ^{o}C) gel" was electrically characterized.

Figure 5b: Scan the voltage from 0 V to 4 V and record the current through fresh regioregular P3HT solution, spontaneously formed gelator by cooling (ca. 4 ^{o}C) and the high-conductivity gelator made by applying a long time of bias voltage (4 V for 36 hours). All the measurements were performed at room temperature (22 ^{o}C).

Figure 5c: The current @ 1V was in-situ detected while the device were immersed into boiling water (ca. 100 ^{o}C) for 90 s and kept in ice/water bath (0 ^{o}C) for 15 min repeatedly. More repeating cycles (108 times) were depicted as Figure S12b. The gel measured at 0 ^{o}C (Figure 5c) is much more conductive than that being measured at 22 ^{o}C (Figure 5b).

Figure 5d: A persistent DC voltage bias of 4 V was applied and we recorded the in-situ current with an interval of 10 seconds. Every 3000 seconds, we would put the device onto a hotplate pre-heated to 85 ^{o}C for 120 seconds and then take it off the hotplate. Several cycles were demonstrated by repeating this process.

3. Supplementary Figures:

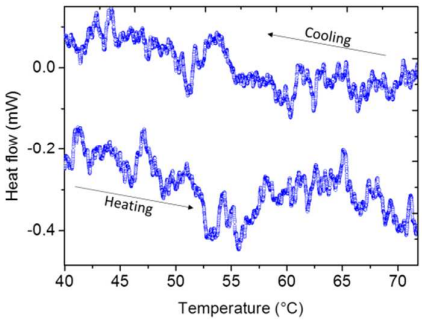

Supplementary Figure 1. No appreciable endothermic or exothermic peaks were observed in differential scanning calorimetry (DSC) characterization.

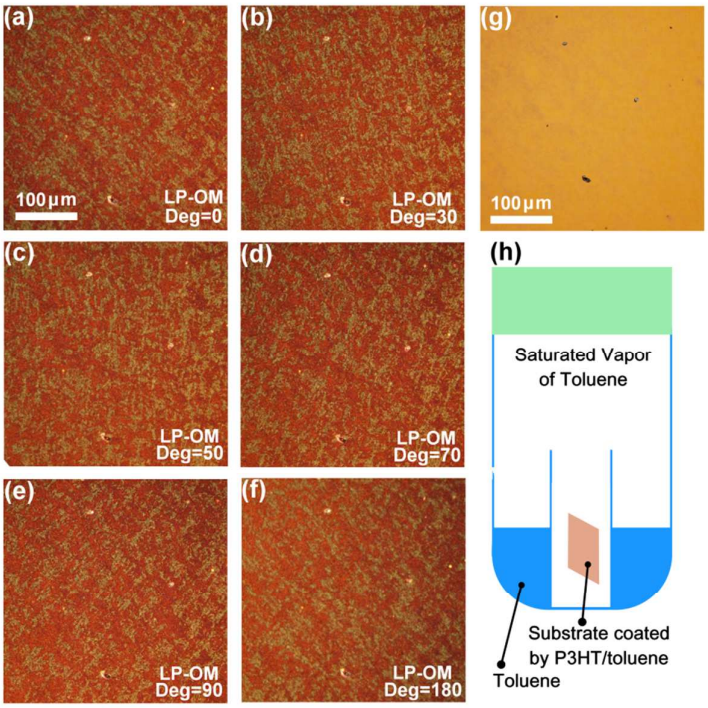

Supplementary Figure 2. (a-f) linearly polarized and (g) optical microscope images of an rr-P3HT aerogel film. (h) Scheme of the method used to prepare aerogel film. In detail, 100 µL of fresh rr-P3HT/toluene solution was dropped onto a substrate, then the substrate was kept vertical in saturated vapor of toluene and put in fridge (ca. 4 ^{o}C). All substrates used for acquiring optical microscope images underwent a 1-day long drying process before being imaged. Previously followed methods to deposit P3HT aerogel film can be found in supplementary reference 1 to 3.

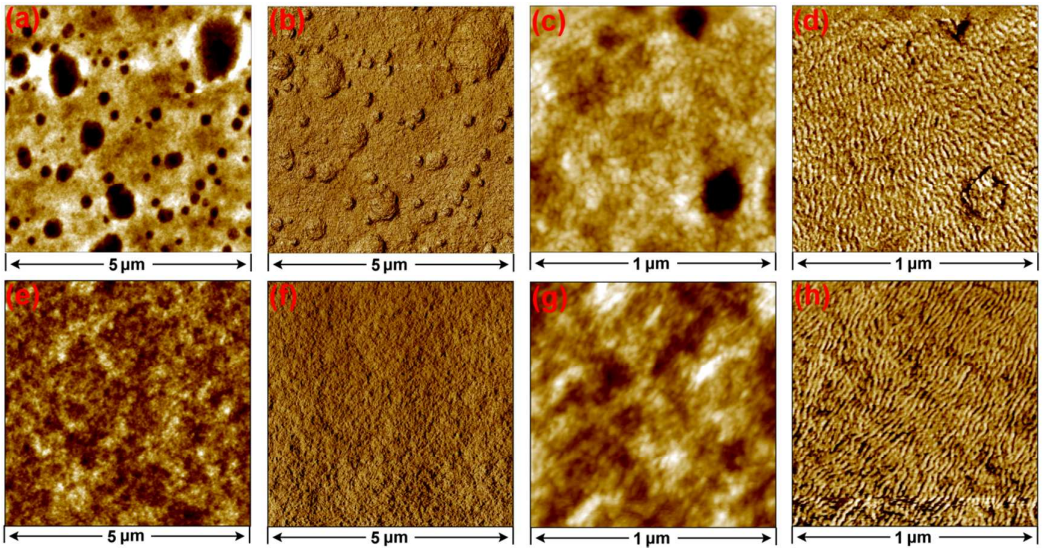

Supplementary Figure 3. Intermittent contact AFM images of the morphology of dry rr-P3HT (Mw=31300 and 55000) gelator films. (a-d) rr-P3HT of Mw=31300, (e-h) rr-P3HT of M_W = 55000. (a, c, e, g) Height images, (b, d, f, h) corresponding phase images. Z-scales of the height images: (a) = 45 nm, (c) = 26 nm, (e) = 26 nm, and (g) = 17 nm. The AFM images, together with the optical microscope images displayed in Figure S2, provide unambiguous evidence for the uniformity of the rr-P3HT aerogel film. The zoom-ins clearly displays the nanofibrillar morphology for both Mw of 55000 and 31300 based films, as portrayed in the subpanels (c-d) and (g-h), respectively. [All substrates used for acquiring AFM images underwent a 1-day long drying process before being imaged (see the method shown in Figure S2)]

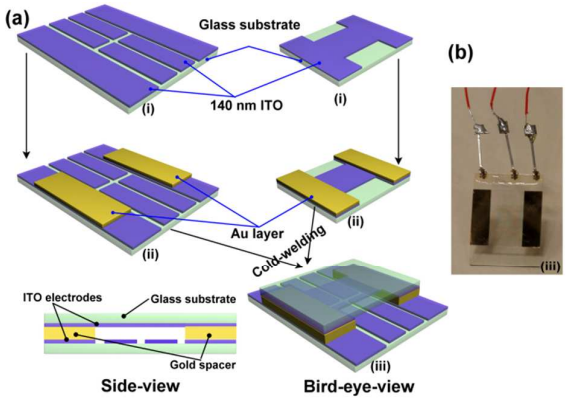

Supplementary Figure 4. (a) Schematic diagram of the device fabrication method of ITO-based electrodic cavity. (i) Two glass substrates exposing 145 nm thick ITO transparent electrodes patterned by photolithography. (ii) Gold pads with different thickness have been deposited by vacuum evaporation through shadow masks. (iii) Two parts of the device are brought together to form an electrodic cavity by means of cold-welding. The side-view schematic diagram shows that the cavity thickness is determined by the Au layer. Here three different cavities have been fabricated with the interelectrodic distance of 100 nm, 250 nm and 550 nm. (b) An exemplary empty sample of ITO-based cavity electrodes. The device is

transparent as a result of the use of ITO as electrode. Noteworthy, the ITO-based electrodic cavity is LiF-spacer-free because cold-welding does not occur in the case of ITO. The device surface area amounts to 2.25 mm^2 (1.5 × 1.5 mm^2).

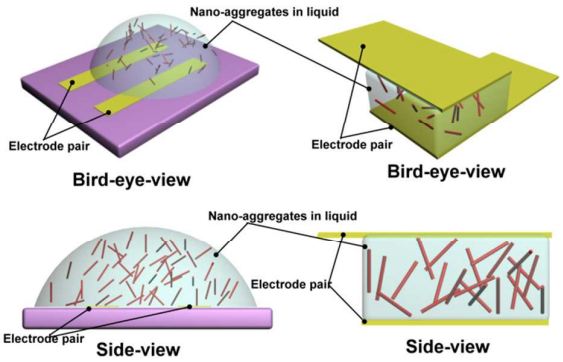

Supplementary Figure 5. Schematic diagram of the device configurations with lateral (left panel) and vertical (right panel) electrodes arrangement. Compared to a more traditional device based on a lateral configuration, our cavity-like electrode provides an ideal platform for testing the nano-aggregates in liquid phase because of the following three reasons: 1) the electrical field would penetrate the liquid rather than concentrating at the interface between electrodes plane and substrate as shown in the left part. 2) Self-encapsulation device structure can protect long-time measurement from the dust being present in the environment. 3) Nano-aggregates inside a cavity can provide more direct pathway for the current flow. As a result, the formation and disappearance of nano-aggregates in the liquid will endow the device more dramatic conductivity changes.

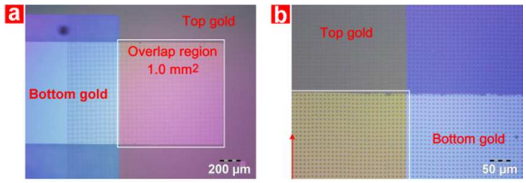

Supplementary Figure 6. (a) The microscopy picture of the device region, which was defined by the overlapping square between top and bottom electrodes (1.0 × 1.0 mm^2). This image also appears as the inset of Figure 3a. (b) Zoom-in of the device region shows LiF pillar array spacers with a periodicity of 10 μm. In the future, water-instable LiF salt could be replaced by inert dielectric materials like SiO_2 if the aqueous phase gelators was used. It is worth noting that in the ITO-based electrodic cavity, LiF spacer layer is not necessary any more.

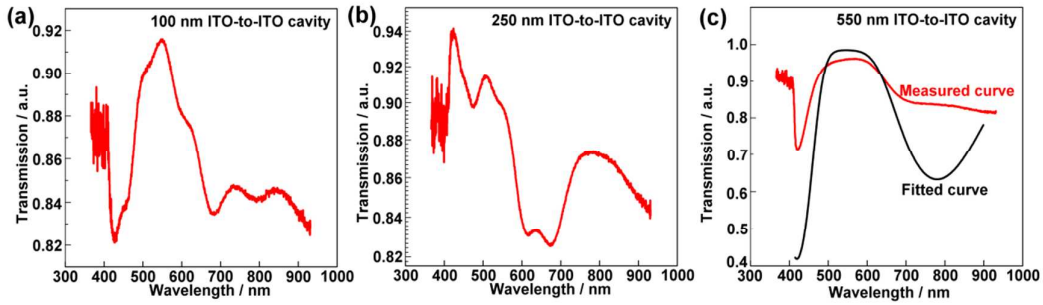

Supplementary Figure 7. Transmission spectra of the ITO-based electrodic cavities with different interelectrodic distance of (a) 100 nm, (b) 250 nm and (c) 550 nm. The cavity length is determined by the thickness of gold layer deposited for cold-welding (Fig. S4). The transmission spectrum provides evidence that ITO-based electrodic cavity is totally transparent to visible light. For the cavity of 550 nm, the transmission spectra measured from the sample were compared to those predicted by transfer matrix calculations. The latter is obtained by solving Maxwell's equations for the multilayer composed of two ITO coated glass substrates separated by an air gap. The predicted transmission spectrum (black curve of Fig. S7 c) displays a broad maximum at ca. 550 nm, in agreement with the measured data, confirming that the cavity length is indeed determined by the thickness of gold layer (to be 550 nm). [In the calculation, the thickness of the ITO layers was set to the value of 145 nm as determined by profilometer and its refractive index was taken from published literature.[4]]

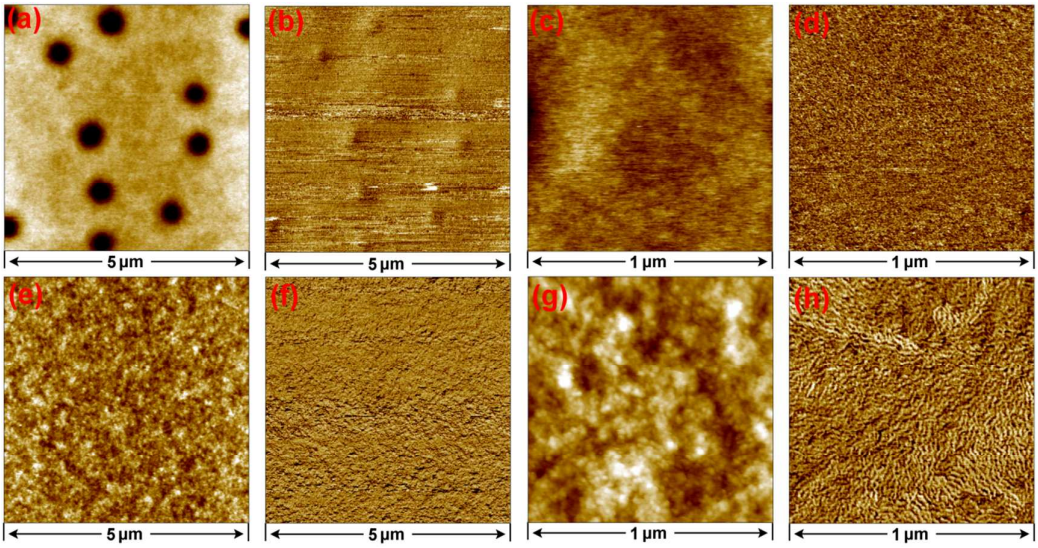

Supplementary Figure 8. Intermittent contact AFM images of the morphology of (a-d) spin-coated RRa-P3HT thin films. (a,c) Height images, (b,d) corresponding phase images. (e,h) Control experiment on rr-P3HT of M_W = 50000 which is deposited also by spin-coating using the same conditions. (e,g) Height images, (f,h) corresponding phase images. The AFM pictures show that regiorandom (RRa-) P3HT does not form nano-fibers when it is dry. As a comparison, rr-P3HT always tends to aggregate into nano-fibers even when the film is prepared by spin-coating. Z-scale in height images: (a) = 9 nm, (c) = 4 nm, (e) = 17 nm, and (g) = 14 nm.

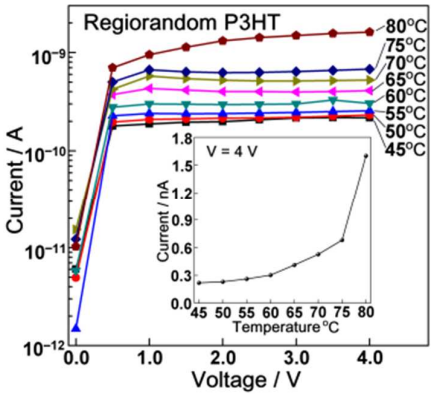

Supplementary Figure 9. Logarithmic *I-V* plots for the electrodic cavity contains RRa-P3HT solution (25 mg/ml). Inset shows current vs. T. variation (bias = 4 V) controlled by a hotplate. More detailed investigation in this regard will require to measure highly diluted solution to exclude molecular interaction. More precise temperature control is also beneficial to make systematic study on *solution conductivity*. However, these efforts are out of our main scope of this study on *gelator conductivity*.

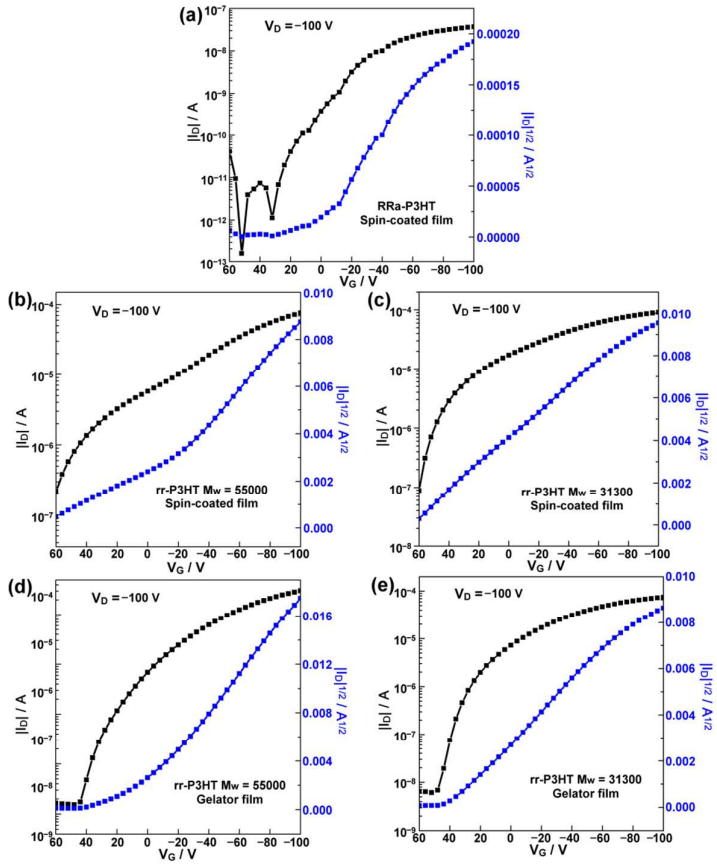

Supplementary Figure 10. Typical transfer curves of the OFETs based on (a) spin-coated RRa-P3HT film, (b) spin-coated rr-P3HT (Mw=55000) film, (c) spin-coated rr-P3HT (Mw=31300) film, (d) rr-P3HT (Mw=55000) gelator film deposited as described in Figure S2 and (e) rr-P3HT (Mw=31300) gelator film drop-casted as shown in Figure S2. All these three P3HT materials

exhibit p-type OFET behavior. The measurements were performed in a glovebox filled with nitrogen. Regiorandom P3HT showed the lowest I_D because the steric repulsion between "head-to-tail" alkyl substituent groups in regiorandom (RRa) P3HT yields a distortion of the molecular backbone, thereby reducing the conjugation length, the molecular planarity and therefore intermolecular π-π stacking.

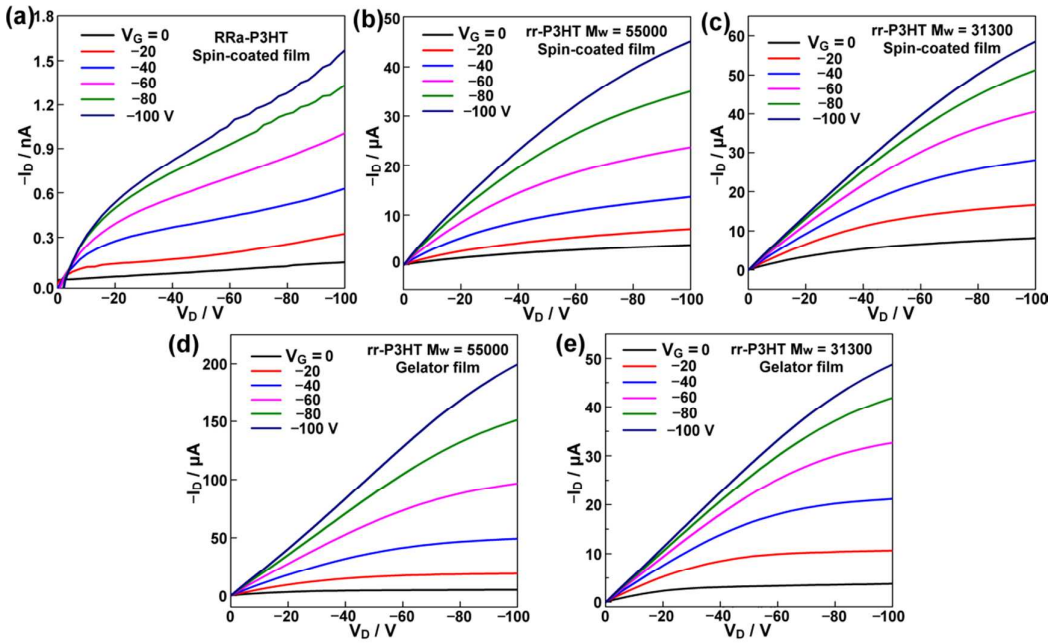

Supplementary Figure 11. Typical output curves of the OFETs based on (a) spin-coated RRa-P3HT film, (b) spin-coated rr-P3HT (Mw=55000) film, (c) spin-coated rr-P3HT (Mw=31300) film, (d) rr-P3HT (Mw=55000) gelator film deposited as described in Figure S2, and (e) rr-P3HT (Mw=31300) gelator film drop-cast as displayed in Figure S2. All these OFETs based on three P3HT materials work in enhancement mode and show a typical gate voltage regulated output current. These measurements were performed in a glovebox filled with nitrogen.

Table S1. The OFETs properties of rr-P3HT with different Mw (31300 and 55000) and RRa-P3HT. These films were prepared by spin-coating. The RRa-P3HT film showed very poor charge carrier mobility values due to its amorphous nature.[5]

Materials	Channel length (μm)	Charge carrier mobility (cm^2/V.s)	V_T (V)	On/off ratio
rr-P3HT 55k	2.5	2.2×10^{-3}	44.5	133
	5.0	1.2×10^{-3}	24.5	207
	10	7.0×10^{-4}	22.1	348
	20	5.1×10^{-4}	21.4	323
rr-P3HT 31k	2.5	9.7×10^{-4}	88.8	60
	5.0	6.4×10^{-4}	76.4	229
	10	4.54×10^{-4}	70.8	965
	20	4.1×10^{-4}	66.1	1050
RRa-P3HT	2.5	7.96×10^{-7}	83	6.41
	5.0	4.85×10^{-7}	57.2	23
	10	6.6×10^{-7}	28	5.4×10^{3}
	20	5.3×10^{-7}	4.3	3.11×10^{3}

Table S2. OFET properties of regioregular P3HT gelator films prepared by the drop-casting method shown in Fig. S2.

Materials	Channel length (μm)	Charge carrier mobility (cm^2/V.s)	V_T (V)	On/off ratio
rr-P3HT 55k	2.5	7.7×10^{-3}	23.5	6.4×10^{4}
	5.0	3.5×10^{-3}	26.9	3.76×10^{4}
	10	4.0×10^{-3}	10.0	1.68×10^{4}
	20	1.45×10^{-3}	20.0	6.0×10^{3}
rr-P3HT 31k	2.5	1.23×10^{-3}	55.0	1.39×10^{3}
	5.0	9.7×10^{-4}	38.6	4.59×10^{3}
	10	6.08×10^{-4}	43	9.5×10^{3}
	20	4.5×10^{-4}	43	3.6×10^{3}

The charge carrier mobility (in saturation region, both here and in Table S1) is higher compared to the films made by spin-coating the identical polymer. This observation is in accordance with the morphology study showing a greater propensity to form fibrillar morphology in drop-cast films. The formation of high-quality nano-fibers provides evidence for the existence of better intermolecular stacking in the case of P3HT materials. Interestingly,

films exhibiting a greater fibrillar morphology display higher charge carrier mobility values when a shorter channel length is employed.

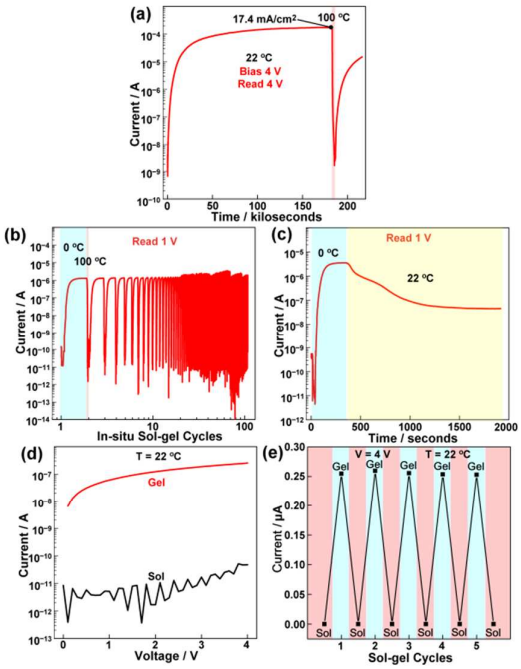

Supplementary Figure 12. (a) The conductivity of rr-P3HT gel can reach a plateau when very long time DC bias is applied (4 V, more than 72 hours). Such a high current density of 17.4 mA/cm^2 could still recover to low-conductivity state by simply heating to 100 °C. (b) Over 100 cycles of repeating heating/cooling procedure were in-situ electrically probed. The sol-gel transition was accompanied by the dramatic conductivity change. (c) The conductivity of spontaneously formed rr-P3HT gel by 0 °C cooling decreases by almost two orders of magnitude when the temperature recovers from 0 °C to room temperature (ca. 22 °C). The gel is highly susceptible by temperature changes. (d) Room temperature I-V curves of the rr-P3HT/toluene system in sol and gel states. (e) The current @4 V of the sol and gel states were plotted by repeating several cycles of sol-gel transition in (d). The difference between the sol-gel transitions depicted by Figure S12e and Figure 4c lies the measurement of Figure S12e was always performed at room temperature.

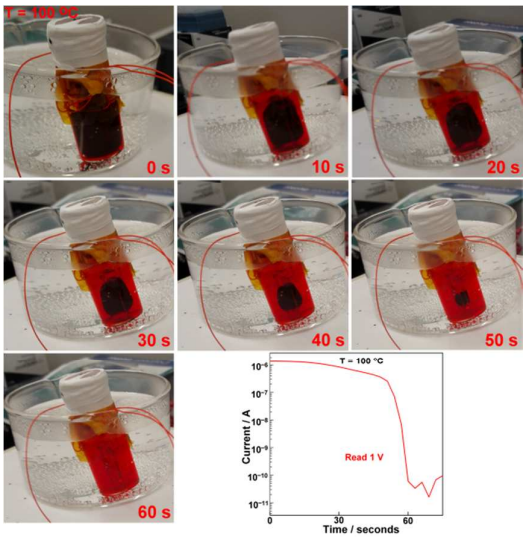

Supplementary Figure 13. When the rr-P3HT gel was placed in a boiling water bath, the gel-sol transition is accompanied with both color and electrical property changes. The conductivity will decrease almost 5 orders of magnitude when the gel vanishes.

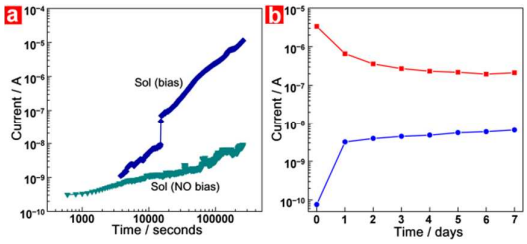

Supplementary Figure 14. (a) Current vs time measurement of the regioregular P3HT solution with and without 4 V DC bias. The condition for the "no bias" electrical measurement was similar to the one we used in Fig. 4d, where the interval time between two sampling points has been prolonged to 200 s and the sensing time has been shrunk to 20 ms in order to minimize the interfering effect brought by the current measurement. Along with increasing bias time, the memory window will widen to more than three orders of magnitude thanks to the upsoaring conductivity upon DC bias. (b) The current variation plotted daily for the high-conductivity state (after days of 4 V bias) and a low-conductivity state (fresh solution without bias) for identical device.

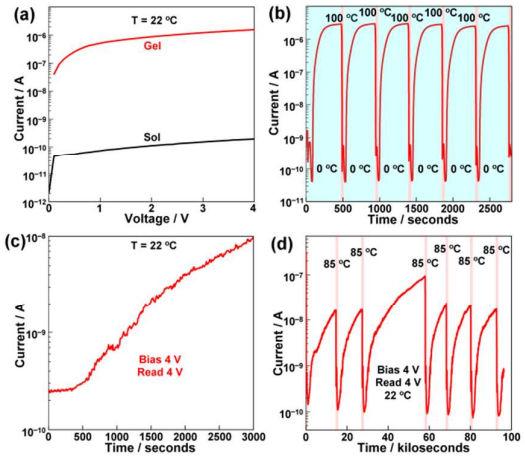

Supplementary Figure 15. The electrical characterization of rr-P3HT (Mw=31300) in sub-micron electrodic cavity. (a) The conductivity of rr-P3HT (Mw=31300) dissolved in toluene could also be tuned for several orders of magnitude by the formation of π-gel (like Figure 4b). (b) In-situ electrical probing of several cycles of sol-gel transition. (c) DC bias could also trigger the formation of gels in the case of rr-P3HT with lower molecular weight. (d) In-situ measuring the current under bias condition. Warming up at 85 ^{o}C for a few minutes could reset the device to the low-conductivity state by breaking down the nanofibers formed upon bias.

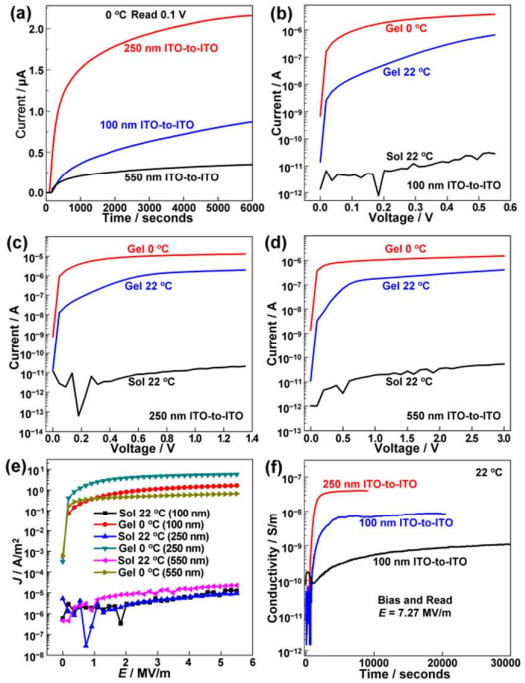

Supplementary Figure 16. The electrical properties of rr-P3HT (Mw=55000) in sol/gel states has also been characterized in the ITO-based electrodic cavity upon varying the interelectrodic distance at 100 nm, 250 nm and 550 nm. (a) In-situ sol-gel transition by cooling down the device to 0 °C and keeping it at such a temperature for tens minutes. The device surface area amounted always to 2.25 mm^2 for the ITO cavity with different

interelectrodic distance. I-V curves of rr-P3HT (Mw=55000) in the ITO-cavity with a distance of (b) 100 nm, (c) 250 nm and (d) 550 nm. (e) The current density (A/m^2) being plotted with the electrical field strength (MV/m) to show the conductivity (S/m) of rr-P3HT gels in different cavity length. It is not surprising that rr-P3HT gels in 250 nm and 100 nm cavities show larger conductivity than in 550 nm cavity thanks to the minimization of inter-fibers connections and associated drop in charge transport. (f) Long time DC bias could also lead to the high-conductivity gel state in the case of ITO-based electrodic cavities. Similarly, the cavity with 250 nm interelectrodic distance shows the best electrical conductivity after DC bias.

4. Supplementary Reference

(1) Lee, C. S.; Yin, W.; Holt, A. P.; Sangoro, J. R.; Sokolov, A. P.; Dadmun, M. D. *Adv. Funct. Mater.* **2015**, *25*, 5848.

(2) Huang, P. T.; Chang, Y. S.; Chou, C. W. *J. Appl. Polym. Sci.* **2011**, *122*, 233.

(3) Kao, K. Y.; Lo, S. C.; Chen, H. L.; Chen, J. H.; Chen, S. A. *J. Phys. Chem. B* **2014**, *118*, 14510.

(4) Moerland, R. J.; Hoogenboom, J. P. *Optica* **2016**, *3*, 112.

(5) Mauer, R.; Kastler, M.; Laquai, F. *Advanced Functional Materials* **2010**, *20*, 2085.